ARTICLE

Self-Assembled Double Ladder Structure Formed Inside Carbon Nanotubes by Encapsulation of $H_8Si_8O_{12}$

Zheng Liu,[†,*] Soon-Kil Joung,[†] Toshiya Okazaki,[†] Kazu Suenaga,[†] Yoshiaki Hagiwara,[‡] Tetsu Ohsuna,[‡] Kazuyuki Kuroda,[‡] and Sumio Iijima[†]

[†]Nanotube Research Center, National Institute of Advanced Industrial Science and Technology (AIST), Tsukuba 305-8565, Japan, and [‡]Department of Applied Chemistry, Faculty of Science and Engineering, Waseda University, Tokyo 169-8555, Japan

ABSTRACT Unique low-dimensional SiO_2-based nanomaterials can be encapsulated and synthesized inside the nanometer-scale one-dimensional internal spaces of carbon nanotubes (CNTs). In this study, various single-walled CNTs (SWNTs) and double-walled CNTs (DWNTs) having different diameters are used as containers for cubic octameric $H_8Si_8O_{12}$ molecules. High-resolution transmission electron microscopy (HRTEM), Fourier transform infrared (FT-IR) spectroscopy, and Raman spectroscopy observations revealed that, depending on the diameter of the CNTs, two types of structures are formed inside the SWNTs and DWNTs: In the case of those CNTs having inner diameters ranging from 1.2 to 1.4 nm, a new ordered self-assembled structure composed of $H_8Si_{4n}O_{8n-4}$ molecules was formed through the transformation of $H_8Si_8O_{12}$; however, in the case of CNTs having inner diameters larger than 1.7 nm, a disordered structure was formed. This behavior may indicate that strong interactions occur between the CNTs and the encapsulated $H_8Si_{4n}O_{8n-4}$ molecules.

KEYWORDS: carbon nanotubes · electron microscopy · octahydridosilsesquioxane · structure evaluation · double ladder structure

Carbon nanotubes (CNTs) are promising candidates for various potential applications. The physical and chemical properties of CNTs can be modified by doping, that is, by introducing various molecules in CNTs.[1−3] There exist unique low-dimensional nanomaterials that can be synthesized and encapsulated inside one-dimensional nanometer-scale internal spaces of CNTs. Low-dimensional metal halides and metal alloy crystals have been synthesized inside single-walled CNTs (SWNTs).[4−6] Metal nanowires have been synthesized inside SWNTs by a nanotemplate reaction.[7,8] Various inorganic oxides have been encapsulated inside SWNTs to form unique low-dimensional structures.[9,10] Hydridosilsesquioxane clusters, $(HSiO_{1.5})_n$ (n = 8, 10, 12, 14), which are well-defined chemical species, have attracted attention for the synthesis of ladder- and cage-shaped polysilsesquioxanes because they consist of unique two- and three-dimensional structures and have potentially better chemical, physical, and electrical properties than those of silicones.[11] Cage-shaped polysilsesquioxanes, particularly cubic-shaped octahydridosilsesquioxane clusters $H_8Si_8O_{12}$, have always generated considerable interest. For example, Schneider *et al.* have investigated the reaction of $H_8Si_8O_{12}$ on Si(1 0 0)-(2 × 1) and Si(1 1 1)-(7 × 7) surfaces by scanning tunneling microscopy (STM), X-ray photoemission, and reflection−absorption infrared (IR) spectroscopy.[12] The monolayer assembly of $H_8Si_8O_{12}$ on freshly evaporated gold surfaces in ultrahigh vacuum has been characterized.[13−16] The layer structure of $H_8Si_8O_{12}$ molecules physisorbed on highly oriented pyrolytic graphite had also been investigated by STM.[17] Recently, Wang *et al.*[18] encapsulated $H_8Si_8O_{12}$ molecules in CNTs by using a pressure-cycling filling technique[19] and studied them by transmission electron microscopy (TEM) and IR spectroscopy. They found that $H_8Si_8O_{12}$ could be efficiently encapsulated in SWNTs having diameters of 1.4−1.5 nm and in multiwalled CNTs having internal diameters of 1.0−3.0 nm; however, ordered structures formed inside CNTs were not observed.[18] The relationship between structures formed inside CNTs and the CNT diameters requires further investigation. In this study, we used various SWNTs and double-walled CNTs (DWNTs) having different diameters as containers for $H_8Si_8O_{12}$ molecules. Through the transformation of $H_8Si_8O_{12}$, a new ordered self-assembled structure was formed in only those SWNTs and DWNTs that had specific diameter distributions (ranging from 1.2 to 1.4 nm), and a disordered structure was formed inside those CNTs that had diameters larger than 1.7 nm. This behavior may indicate that strong interactions occur between the CNTs and the encapsu-

*Address correspondence to liu-z@aist.go.jp.

Received for review July 16, 2008 and accepted April 23, 2009.

Published online May 1, 2009.
10.1021/nn9002727 CCC: $40.75

lated molecules that have an ordered structure. High-resolution TEM (HRTEM), with a point resolution of 0.14 nm, IR spectroscopy, and Raman spectroscopy were used for demonstrating the formation of the new structure.

RESULTS AND DISCUSSION

Figure 1a shows an ordinary $H_8Si_8O_{12}$ molecular structure not encapsulated inside CNTs after the geometrical optimization by using the density functional theory (DFT) method. The Si−Si distances (d_{Si-Si}) are 0.3117, 0.3116, and 0.3128 nm in the *x*, *y*, and *z* directions, respectively. These values are different from that in the case of $H_8Si_8O_{12}$ crystals, where $d_{Si-Si} = 0.3121$ nm.[20] It can be seen that the $H_8Si_8O_{12}$ molecular structure has a slight deviation from the cubic structure in the crystal state.

A rather interesting phenomenon was observed when $H_8Si_8O_{12}$ molecules were encapsulated inside CNTs. $H_8Si_8O_{12}$ molecules were always arranged in an ordered compact chain form in the CNTs having specific diameters distributions (ranging from 1.2 to 1.4 nm, as discussed below), as shown in Figure 2; the black dots in the HRTEM image correspond to Si atoms inside the SWNT. However, the distance between two neighboring Si atoms in the chain along the transverse axis direction of the CNTs was not constant (varying from 0.282 to 0.292 nm) and was shorter than that calculated from the lattice parameter values of the ordinary $H_8Si_8O_{12}$ molecular structure. Furthermore, the distance between Si atoms in the vertical axis direction of the CNTs was also not constant (varying from 0.305 to 0.329 nm); this indicates that the bond angles of Si−O−Si in the chain were not uniform. These significant results show that, when the $H_8Si_8O_{12}$ molecules were encapsulated in the CNTs, their structure transformed from the original structure (isolated molecule) to a polymerized structure. Besides these ordered structures, a disordered structure was also observed inside the CNTs having larger diameters, as shown in Figure S1 in Supporting Information. The IR and Raman studies, which were conducted prior to the HRTEM observation, also revealed the formation of the new structure; this implied that the new structure was not formed due to the electron beam used in the HRTEM observation. Additionally, by using HRTEM, we observed a mixture of open-ended CNTs and $H_8Si_8O_{12}$ molecules dissolved in hexane without ultrasonication, and we also found that this new self-assembled structure formed inside the CNTs having specific diameters (ranging from 1.2 to 1.4 nm). Consequently, we inferred that the new structure was not formed by ultrasonication. The ordered and disordered structures were formed selectively inside CNTs having different diameters, suggesting that the diameter of CNTs may be a crucial factor in their formation. As discussed later, the formation of this new structure does not depend on whether the CNT is metallic or semiconducting. Two chain structures of $H_{2n+4}Si_{2n}O_{3n-2}$ and $H_8Si_{4n}O_{8n-4}$ are assumed through the transformation of $H_8Si_8O_{12}$ molecules by losing H atoms and the connecting of two Si atoms in the neighboring $H_8Si_8O_{12}$ molecules through an O atom. These structures are shown in Figure 1b,c after geometrical optimization by the DFT method. The chain structure of $H_{2n+4}Si_{2n}O_{3n-2}$ is supposed to be a ladder structure and that of $H_8Si_{4n}O_{8n-4}$ should be a double ladder structure.

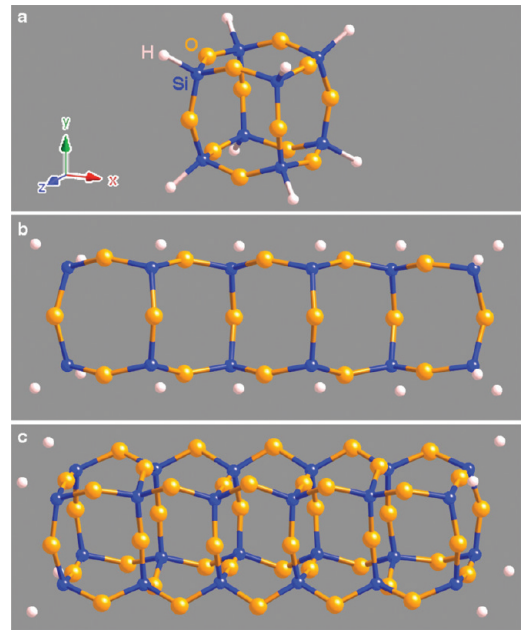

Figure 1. Ordinary $H_8Si_8O_{12}$ structure after geometrical optimization (a), a ladder structure of $H_{2n+4}Si_{2n}O_{3n-2}$ (b), and a double ladder structure $H_8Si_{4n}O_{8n-4}$ (c).

A Si $L_{2,3}$ core-loss edge can be used to probe the crystal chemistry around Si.[21] Electron energy loss spectroscopy (EELS) analysis also revealed the structural deviation from the original $H_8Si_8O_{12}$ crystal structure after the encapsulation of the $H_8Si_8O_{12}$ molecules inside SWNTs; this behavior can be observed from the peak shift of the Si $L_{2,3}$ edge toward the direction of lower energy by approximately 1 eV. This indicates that the local chemical states around Si atoms vary as shown in Figure S2 in Supporting Information.

Figure 3a shows a part of the HRTEM image of $H_8Si_8O_{12}$ encapsulated inside the HiPCO SWNT shown in Figure 2a, along with simulated images of both $H_8Si_{4n}O_{8n-4}$ and $H_{2n+4}Si_{2n}O_{3n-2}$ structures inside the SWNT. Here, we call the orientation of such an arrangement as being in the <100> direction. A line profile analysis of the image was carried out in order to compare the two above-mentioned structures. In order to make an accurate quantitative comparison, we determined that the chiral index of the SWNT in the HRTEM image was (14,2) through Fourier transformation of the HRTEM image and from the diameter of the SWNT; this indicates that it is a metallic CNT.[22,23] Furthermore,

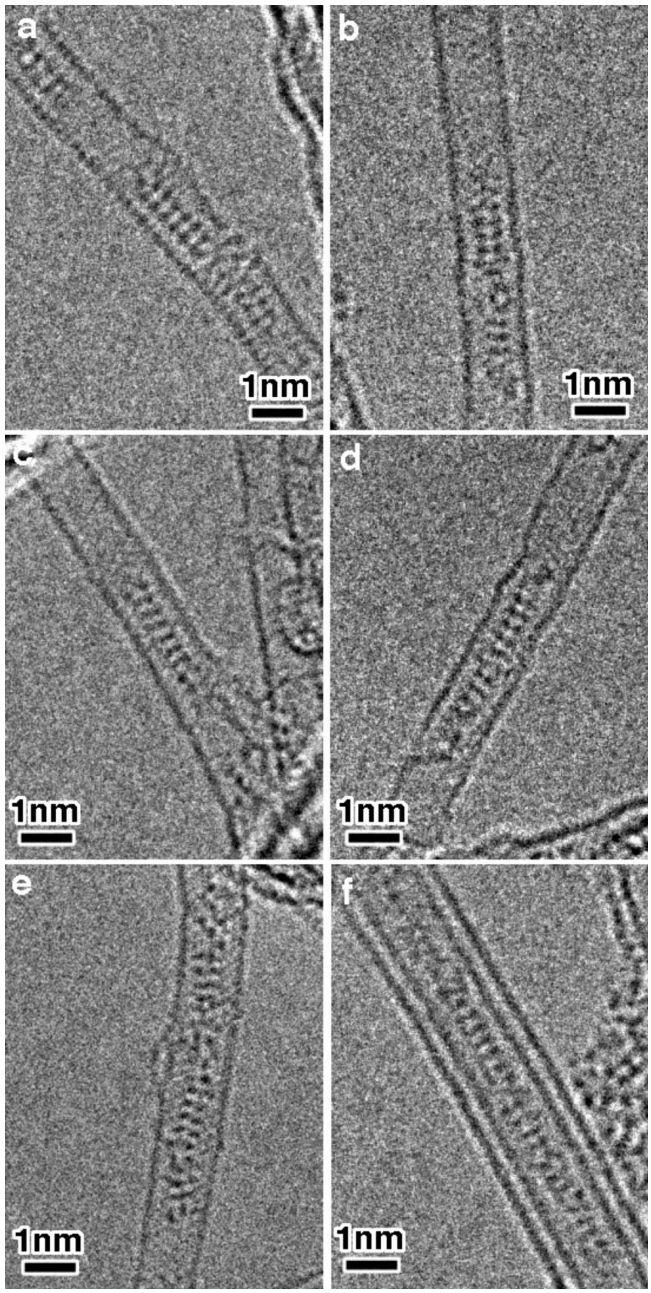

Figure 2. HRTEM images of $H_8Si_8O_{12}$ encapsulated inside the various CNTs. (a−d) HRTEM images of $H_8Si_8O_{12}$@HiPCO SWNTs, (e) HRTEM image of $H_8Si_8O_{12}$@FH-P SWNT, (f) HRTEM image of $H_8Si_8O_{12}$@FH-P DWNT.

the positions of Si atoms along the longitudinal direction relative to the SWNT were also considered in the simulation by comparing the positions of Si atoms through comparing the 2.14 Å periodicity dot contrast of C atoms in the wall of the SWNT in the HRTEM image. The simulated images shown in Figure 3b,c were obtained under identical defocus conditions according to that observed in the actual HRTEM image. It should be noted that, in the line profiles shown in Figure 3d−f, the contrasts of Si atoms are darker than those of the walls of the SWNT in the HRTEM image; furthermore, the contrast ratios of Si atoms to the SWNT wall in the line profile of the HRTEM image are in excellent agreement with those in the line profile of the simulated image obtained by assuming the double ladder structure of $H_8Si_{4n}O_{8n-4}$. On the contrary, the contrast of Si atoms is clearly lighter than that of the SWNT wall in the line profile in the simulated image obtained by assuming the single ladder structure of $H_{2n+4}Si_{2n}O_{3n-2}$. Figure 3g−i shows the comparison between the HRTEM image and the simulated image of the $H_8Si_{4n}O_{8n-4}$ structure inside the (14,2) SWNT. The simulated structure with the $H_8Si_{4n}O_{8n-4}$ molecules inside the (14,2) SWNT has been geometrically optimized by using molecular mechanics with the MM+ force field method. From the overlap of the HRTEM image and simulated image, it can be observed that there is a good agreement between the images in terms of the contrast of the Si atoms in both the [010] and [001] directions. From these results, it can be deduced that the $H_8Si_{4n}O_{8n-4}$ structure is the most suitable and probable candidate for the new structure that is formed inside the SWNT.

In addition to observing the arrangement of the $H_8Si_{4n}O_{8n-4}$ structure in the <100> direction, its arrangement was also observed in the <110> direction, as shown in Figure 4. The simulated image, the overlap of the simulated image with the HRTEM image, and the model of the $H_8Si_{4n}O_{8n-4}$ structure inside the SWNT in the <110> direction are also shown in this figure. The chiral index of the SWNT in the HRTEM image was determined as (13,5)—a semiconducting CNT; this chiral index value was used in the simulation. The structure of $H_8Si_{4n}O_{8n-4}$ molecules inside the (13,5) SWNT was geometrically optimized before it was used in the simulation. In this case, the overlap of the simulated image with the HRTEM image also resulted in a good fit. By comparing the line profiles shown in Figure 4c with that in the simulated image shown in Figure 4d, it can be definitely deduced that the contrast of the double Si atoms, which are overlapped along the incident electron beam direction, indicated by the arrows shown by Si(2) existing in the middle of the two single Si atoms shown by Si(1) was just corresponding to the <110> projected direction of the $H_8Si_{4n}O_{8n-4}$ structure.

In the Fourier transform IR (FT-IR) spectrum of $H_8Si_8O_{12}$ crystals, peaks occurring at 861, 1117, and 2291 cm^{-1} can be assigned to the δ(O−Si−H), ν_{as}(Si−O−Si), and ν(Si−H) vibration modes of the $H_8Si_8O_{12}$ crystal,[24] respectively (Figure 5). However, the peak positions of ν_{as}(Si−O−Si) and ν(Si−H) in the spectrum of SWNTs that encapsulated $H_8Si_{4n}O_{8n-4}$ molecules shifted significantly to lower frequencies (−11 and −21 cm^{-1} in the cases of ν_{as}(Si−O−Si) and ν(Si−H), respectively) as compared to those of the original $H_8Si_8O_{12}$ crystal; in contrast, the peak position of δ(O−Si−H) did not change significantly. This behavior demonstrates the transformation of the original structure of the $H_8Si_8O_{12}$ crystal after being encapsulated in-

side the SWNTs and also the strong interaction between SWNTs and the encapsulated $H_8Si_{4n}O_{8n-4}$.

Both of the HRTEM images in the <100> and <110> directions show the new structure of $H_8Si_{4n}O_{8n-4}$ self-assembled inside the SWNTs, although such a structure cannot be observed outside the SWNTs. Furthermore, it should be noted that, although CNTs with different diameters were used in this study, the ordered $H_8Si_{4n}O_{8n-4}$ structure was found to be encapsulated only in those SWNTs that had a diameter distribution in the range of around 1.14−1.31 nm or inside those DWNTs that had an inner tube diameter of approximately 1.15−1.37 nm.

Similar diameter dependences were also observed in the results of resonance Raman spectroscopy (Figure S3 in Supporting Information). The radial breathing mode (RBM) of SWNTs is potentially useful for monitoring tube-specific effects because its frequency almost scales with the inverse of the tube diameter ($1/d_t$) and is sensitive to ambient environments. Figure S3 in Supporting Information shows that the RBMs at 177 and 195 cm^{-1} were shifted to 174 and 192 cm^{-1}, respectively, whereas there was no frequency shift for the RBM at 262 cm^{-1}. According to a previous RBM result,[25] the RBMs at 177, 195, and 262 cm^{-1} can be assigned to SWNTs having d_t = 1.4, 1.2, and 0.9 nm, respectively. This suggests that $H_8Si_{4n}O_{8n-4}$ molecules are preferentially encapsulated in SWNTs having d_t = 1.2−1.4 nm and that the filling of these SWNTs causes their RBM to shift due to the strong interaction between the SWNTs and the $H_8Si_{4n}O_{8n-4}$ molecules. It can be presumed that a diameter of 0.9 nm is too small to encapsulate $H_8Si_{4n}O_{8n-4}$ molecules. The diameter dependence results of HRTEM and Raman spectroscopy match perfectly.

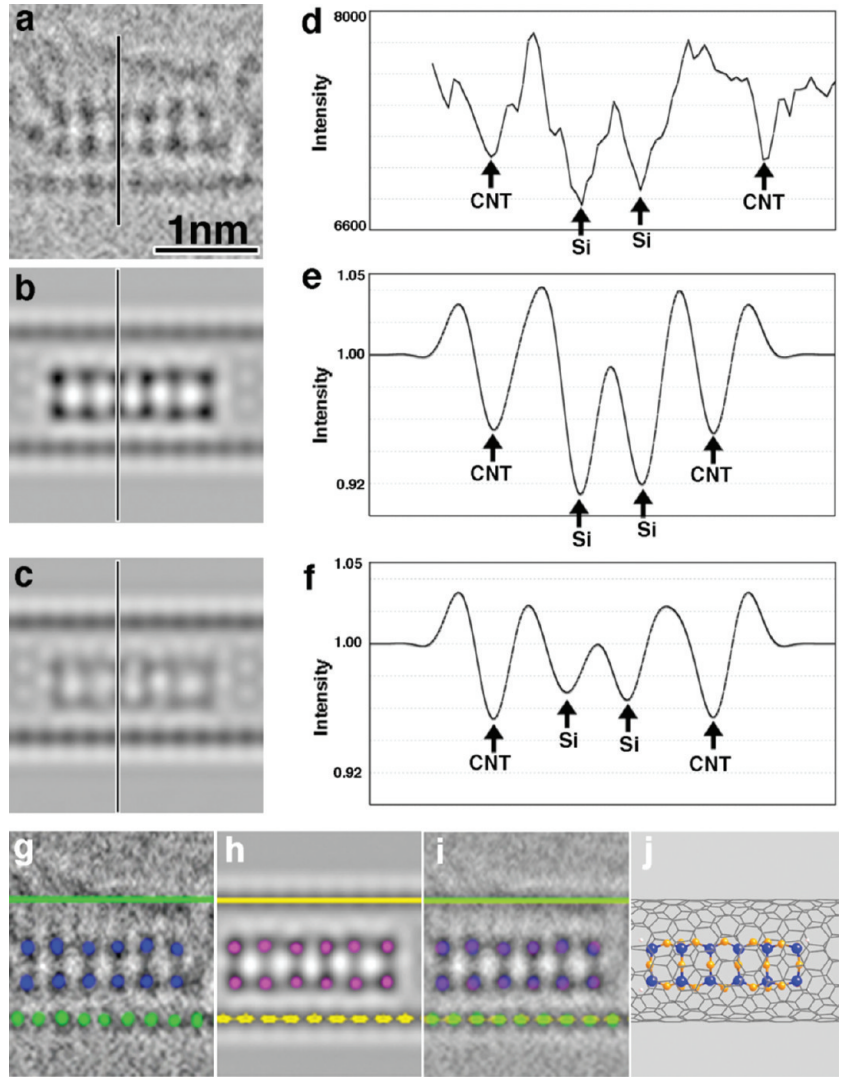

Figure 3. HRTEM image of $H_8Si_8O_{12}$ encapsulated inside the (14,2) SWNT (a), simulated image of the double ladder structure $H_8Si_{4n}O_{8n-4}$ inside the (14,2) SWNT (b), single ladder structure $H_8Si_{2n}O_{3n-2}$ structures inside the (14,2) SWNT (c), and their corresponding line profiles (d−f). HRTEM image of (a) in which the Si atoms and the CNT wall are highlighted (g), simulated image of $H_8Si_{4n}O_{8n-4}$ at (14,2) in which the Si atoms and the CNT wall are highlighted (h), (i) is the overlap of the images (g) and (h), and the framework model of $H_8Si_{4n}O_{8n-4}$ at (14,2) (j).

The diameter of CNTs plays an important role in the formation of the new ordered structure. With losing H atoms, this structure is quite different from that of the original $H_8Si_8O_{12}$ molecules, and for its formation, strong interactions with the walls of the CNTs may be required. It can be seen that CNTs do have robust interactions with the new ordered double ladder structure of $H_8Si_{4n}O_{8n-4}$ formed inside them. In this study, the formation energies of the $H_8Si_{4n}O_{8n-4}$ structure (where n = 6) and of the $H_8Si_8O_{12}$ structure having three unit cells were calculated using the DFT method; both these systems had an equal number of H, Si, and O atoms. The formation energy of the $H_8Si_{4n}O_{8n-4}$ (n = 6) structure was 1.27 hartree (34.792 eV) lower than that of the $H_8Si_8O_{12}$ structure having three unit cells (1.27 hartree corresponds to 5.7 times the average bond energy of O−H bonds in H_2O). Therefore, the $H_8Si_{4n}O_{8n-4}$ structure appears to be more stable than the $H_8Si_8O_{12}$ structure while being encapsulated inside SWNTs.

The new structure of $H_8Si_{4n}O_{8n-4}$ inside the SWNT exhibits double-four-ring (D4R) units[26] of Si−O, which are very important in materials such as zeolites. In this study, the double-five-ring (D5R) structure was also observed in some cases. The arrow in Figure 6 clearly shows a D5R structure existing in the chain between the D4Rs of the $H_8Si_{4n}O_{8n-4}$ structure. The D5R was connected to the D4R through a vertex. The formation of the D5R structure was initially considered due to an impurity consisting of $H_{10}Si_{10}O_{15}$ clusters that might have

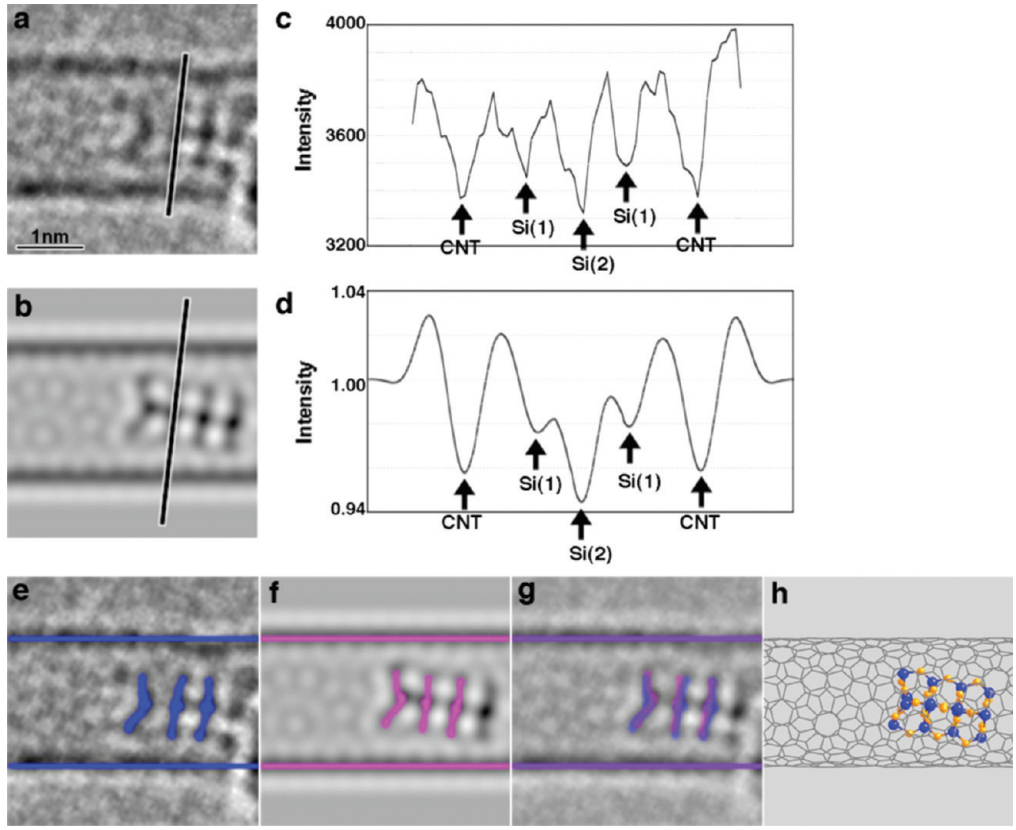

Figure 4. HRTEM image taken from the <110> direction of $H_8Si_{4n}O_{8n-4}$ at (13,5) (a), the corresponding simulated image of $H_8Si_{4n}O_{8n-4}$ at (13,5) (b), and the corresponding line profiles (c,d). HRTEM image of (a) in which the Si atoms and the CNT wall are highlighted (e), the corresponding simulated image of $H_8Si_{4n}O_{8n-4}$ at (13,5) in which the Si atoms and the CNT wall are highlighted (f), (g) is the overlap of the images (e) and (f), and the framework model of $H_8Si_{4n}O_{8n-4}$ @ (13,5) projected from the <110> direction (h).

been mixed in the source $H_8Si_8O_{12}$ powders. However, liquid state NMR data of the original powders show only very minor signals due to the impurity. Therefore, the possibility of the cleavage of the cubic octameric siloxane bond forming new Si−O−Si bonds with neighboring cleaved groups cannot be excluded.

In this study, SWNTs were successfully used as containers in the synthesis of new low-dimensional nanomaterials that do not exist outside CNTs. A new ordered self-assembled structure composed of $H_8Si_{4n}O_{8n-4}$ molecules was formed inside SWNTs and DWNTs having specific diameters sizes (1.2−1.4 nm) through the transformation of $H_8Si_8O_{12}$. However, disordered structures were formed inside those CNTs that had diameters larger than 1.7 nm. This indicates that strong interactions occur between the CNTs and the encapsulated $H_8Si_{4n}O_{8n-4}$ molecules.

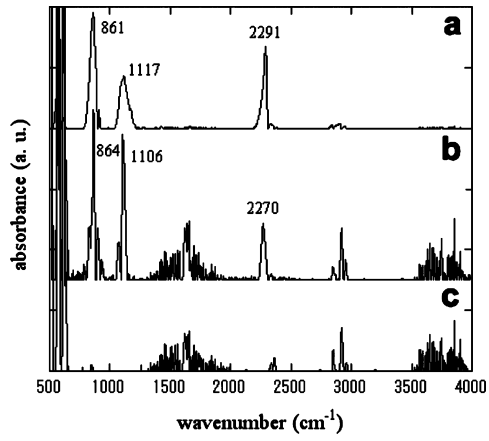

Figure 5. FT-IR spectra of $H_8Si_8O_{12}$ crystal (a) and HiPCO-SWNTs encapsulating $H_8Si_{4n}O_{8n-4}$ molecules (b), together with a reference spectrum of SWNTs control sample (c).

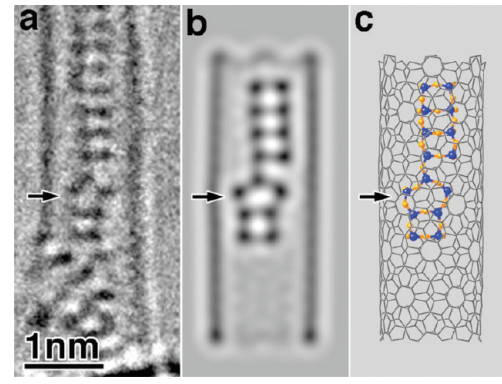

Figure 6. HRTEM image showing the D5R structure existing in between the D4Rs of $H_8Si_{4n}O_{8n-4}$ at (12,6) (a), simulated image (b), and the corresponding framework model (c).

METHODS

In this study, commercially available HiPCO SWNTs (Carbon Nanotechnologies, diameter distribution of around 0.6−1.3 nm) and FH-P SWNTs and FH-P DWNTs (Meijo Nano Carbon Co. Ltd., both having diameter distributions of around 0.9−4.0 nm) were used as containers for $H_8Si_8O_{12}$. Prior to encapsulating $H_8Si_8O_{12}$ inside CNTs, SWNTs and DWNTs were oxidized in air at 500 and 530 °C, respectively, for 30 min in order to open the caps of the nanotubes and to remove amorphous carbon around their surfaces. $H_8Si_8O_{12}$ crystals were first dissolved in hexane (the ratio of $H_8Si_8O_{12}$ to hexane was 0.37 wt %) and then mixed with the cap-opened HiPCO and FH-P CNTs (the ratio of CNTs to $H_8Si_8O_{12}$ was 10 wt %) with and without ultrasonication at room temperature. The mixtures of $H_8Si_8O_{12}$ and CNTs (*i.e.*, the specimens of CNTs encapsulating $H_8Si_8O_{12}$ crystals) were washed more than 10 times with hexane in order to remove $H_8Si_8O_{12}$ crystals surrounding the CNTs prior to FT-IR and Raman measurements. Then, the resulting suspension was placed on a carbon microgrid for TEM observation. The JEM-2010F (JEOL) field emission TEM equipped with a CEOS postspecimen spherical aberration corrector (C_s corrector) was operated at 80 and 120 kV for HRTEM imaging and acquiring electron energy-loss spectra with high resolution and high contrast so that the electron beam damage to the specimen was minimized as much as possible (in this study, the beam density during the observations of the new material synthesized inside CNTs was approximately 120 000 electrons/($nm^2 \cdot s$) or 1.9 C/($cm^2 \cdot s$)). However, we found that the encapsulated ordered structure was destroyed more rapidly under the operation carried out at 80 than at 120 kV when using the same incident beam density. This is due to the radiation damage caused by radiolysis; therefore, the observation condition of an operating voltage of 120 kV is more suitable in this case. Consequently, the results shown in this study were obtained under the observation condition of an operating voltage of 120 kV. The specimens were maintained at ambient temperature during the observation. A Gatan 894 CCD camera was used for digital recording of the HRTEM images. C_s was set in the range of 1−5 μm, and the HRTEM images were recorded under a slightly underfocus condition in order to enhance the contrast of the encapsulated materials with respect to the graphene network of CNTs; this ensured that the contrast of CNTs could be minimized by fabricating the desirable contrast transfer function (CTF).[27] Parallel EELS was carried out using JEM-2010F. The Si $L_{2,3}$ core-loss edge (around 99 eV) was analyzed instead of the O *K*-edge (around 532 eV) because the signal-to-noise ratio in the case of the former was better than that in the case of the latter. FT-IR spectroscopy was carried out by using a Vertex 80v FT-IR spectrometer (Bruker Optics). Nanotube samples were dispersed in ethanol and sprayed onto a ZnSe substrate. Raman spectroscopy was carried out by using a triple-grating monochromator (Bunko-Keiki, BRM-900) equipped with an InGaAs diode array (Princeton Instruments, OMA-V). The Raman spectra were obtained from solid-state samples by using a tunable Ti-sapphire laser (Spectra Physics, 3900S) with an excitation wavelength of 1000 nm. All FT-IR and Raman measurements were performed at room temperature. HRTEM simulations were performed on the simulated structure in the case of molecules inside SWNTs after the structure was geometrically optimized through molecular mechanics with the MM+ force field method.[28,29]

Acknowledgment. This work is partially supported by CREST and Grant-in-Aid from MEXT (19054017). K.K. acknowledges the support by a Grant-in-Aid Scientific Research on Priority Areas "New Materials Science Using Regulated Nano Spaces, Strategy in Ubiquitous Elements" from MEXT, Japan.

Supporting Information Available: Figures S1−S3. This material is available free of charge *via* the Internet at http://pubs.acs.org.

REFERENCES AND NOTES

1. Lee, J.; Kim, H.; Kahng, S.-J.; Kim, G.; Son, Y.-W.; Ihm, J.; Kato, H.; Wang, Z. W.; Okazaki, T.; Shinohara, H.; Kuk, Y. Bandgap Modulation of Carbon Nanotubes by Encapsulated Metallofullerenes. *Nature* **2002**, *415*, 1005–1008.
2. Hornbaker, D. J.; Kahng, S.-J.; Misra, S.; Smith, B. W.; Johnson, A. T.; Mele, E. J.; Luzzi, D. E.; Yazdani, A. Mapping the One-Dimensional Electronic States of Nanotube Peapod Structures. *Science* **2002**, *295*, 828–831.
3. Pichler, T.; Kuzmany, H.; Kataura, H.; Achiba, Y. Metallic Polymers of C_{60} Inside Single-Walled Carbon Nanotubes. *Phys. Rev. Lett.* **2001**, *87*, 267401.
4. Meyer, R. R.; Sloan, J.; Dunin-Borkowski, R. E.; Kirkland, A. I.; Novotny, M. C.; Bailey, S. R.; Hutchison, J. L.; Green, M. L. H. Discrete Atom Imaging of One-Dimensional Crystals Formed within Single-Walled Carbon Nanotubes. *Science* **2000**, *289*, 1324–1326.
5. Carter, R.; Sloan, J.; Kirkland, A. I.; Meyer, R. R.; Lindan, P. J. D.; Lin, G.; Green, M. L. H.; Vlandas, A.; Hutchison, J. L.; Harding, J. Correlation of Structural and Electronic Properties in a New Low-Dimensional Form of Mercury Telluride. *Phys. Rev. Lett.* **2006**, *96*, 215501.
6. Guan, L. H.; Suenaga, K.; Shi, Z.; Gu, Z. N.; Iijima, S. Polymorphic Structures of Iodine and Their Phase Transition in Confined Nanospace. *Nano Lett.* **2007**, *7*, 1532–1535.
7. Kitaura, R.; Imazu, N.; Kobayashi, K.; Shinohara, H. Fabrication of Metal Nanowires in Carbon Nanotubes *via* Versatile Nano-Template Reaction. *Nano Lett.* **2008**, *8*, 693–699.
8. Guan, L. H.; Suenaga, K.; Okubo, S.; Okazaki, T.; Iijima, S. Metallic Wires of Lanthanum Atoms Inside Carbon Nanotubes. *J. Am. Chem. Soc.* **2008**, *130*, 2162–2163.
9. Monthioux, M.; Flahaut, E.; Cleuziou, J.-P. Hybrid Carbon Nanotubes: Strategy, Progress, and Perspectives. *J. Mater. Res.* **2006**, *21*, 2774–2793.
10. Sloan, J.; Matthewman, G.; Dyer-Smith, C.; Sung, A.-Y.; Liu, Z.; Suenaga, K.; Kirkland, A. I.; Flahaut, E. Direct Imaging of the Structure, Relaxation, and Sterically Constrained Motion of Encapsulated Tungsten Polyoxometalate Lindqvist Ions within Carbon Nanotubes. *ACS Nano* **2008**, *2*, 966–976.
11. Gunji, T.; Sopyan, I.; Abe, Y. Synthesis of Polytitanosiloxanes and Their Transformation to SiO_2-TiO_2 Ceramic Fibers. *J. Polym. Sci., Part A* **1994**, *32*, 3133–3139.
12. Schneider, K. S.; Nicholson, K. T.; Owens, T. M.; Orr, B. G.; Banaszak Holl, M. M. The Differential Reactivity of Octahydridosilsesquioxane on Si(1 0 0)-2 × 1 and Si(1 1 1)-7 × 7: A Comparative Experimental Study. *Ultramicroscopy* **2003**, *97*, 35–45.
13. Nicholson, K. T.; Zhang, K. Z.; Banaszak Holl, M. M. Chemisorption of $H_8Si_8O_{12}$ Clusters on Gold: A Novel Si−H Bond Activation. *J. Am. Chem. Soc.* **1999**, *121*, 3232–3233.
14. Nicholson, K. T.; Zhang, K. Z.; Banaszak Holl, M. M.; McFeely, F. R.; Pernisz, U. C. The Dynamic Nature of Hydridosilsesquioxane Clusters on Gold Surfaces. *Langmuir* **2000**, *16*, 8396–8403.
15. Schneider, K. S.; Nicholson, K. T.; Fosnacht, D. R.; Orr, B. G.; Banaszak Holl, M. M. Effect of Surface Reconstruction on Molecular Chemisorption: A Scanning Tunneling Microscopy Study of $H_8Si_8O_{12}$ Clusters on Au(111) $23\times\sqrt{3}$. *Langmuir* **2002**, *18*, 8116–8122.
16. Schneider, K. S.; Nicholson, K. T.; Fosnacht, D. R.; Orr, B. G.; Banaszak Holl, M. M. Chemical Imaging of Terrace-Based Active Sites on Gold. *Langmuir* **2004**, *20*, 2250–2256.
17. Shieh, D. L.; Chen, F. C.; Lin, J. L. Investigation of Orientation and Packing of $H_8Si_8O_{12}$ Arrays on Graphite by Scanning Tunneling Microscopy. *Appl. Surf. Sci.* **2006**, *252*, 2171–2177.
18. Wang, J.; Kuimova, M. K.; Poliakoff, M.; Briggs, G. A. D.; Khlobystov, A. N. Encapsulation and IR Probing of Cube-Shaped Octasilasesquioxane $H_8Si_8O_{12}$ in Carbon Nanotubes. *Angew. Chem., Int. Ed.* **2006**, *45*, 5188–5191.
19. Khlobystov, A. N.; Britz, D. A.; Wang, J.; O'Neil, S. A.; Poliakoff, M.; Briggs, G. A. D. Low Temperature Assembly of Fullerene Arrays in Single-Walled Carbon Nanotubes

Using Supercritical Fluids. *J. Mater. Chem.* **2004**, *14*, 2852–2857.
20. Törnroos, K. W. Octahydridosilasesquioxane Determined by Neutron Diffraction. *Acta Crystallogr., Sect. C* **1994**, *50*, 1646–1648.
21. Garvie, L. A. J.; Buseck, P. R. Bonding in Silicates: Investigation of the Si $L_{2,3}$ Edge by Parallel Electron Energy-Loss Spectroscopy. *Am. Mineral.* **1999**, *84*, 946–964.
22. Hashimoto, A.; Suenaga, K.; Urita, K.; Shimada, T.; Sugai, T.; Bandow, S.; Shinohara, H.; Iijima, S. Atomic Correlation Between Adjacent Graphene Layers in Double-Wall Carbon Nanotubes. *Phys. Rev. Lett.* **2005**, *94*, 045504.
23. Liu, Z.; Suenaga, K.; Yoshida, H.; Sugai, T.; Shinohara, H.; Iijima, S. Determination of Optical Isomers for Left-Handed or Right-Handed Chiral Double-Wall Carbon Nanotubes. *Phys. Rev. Lett.* **2005**, *95*, 187406.
24. Marcolli, C.; Lainé, P.; Bühler, R.; Calzaferri, G.; Tomkinson, J. Vibrations of $H_8Si_8O_{12}$, $D_8Si_8O_{12}$, and $H_{10}Si_{10}O_{15}$ As Determined by INS, IR, and Raman Experiments. *J. Phys. Chem. B* **1997**, *101*, 1171–1179.
25. Weisman, R. B.; Bachilo, S. M. Dependence of Optical Transition Energies on Structure for Single-Walled Carbon Nanotubes in Aqueous Suspension: An Empirical Kataura Plot. *Nano Lett.* **2003**, *3*, 1235–1238.
26. Liu, Z.; Ohsuna, T.; Terasaki, O.; Camblor, M. A.; Diaz-Cabañas, M.-J.; Hiraga, K. The First Zeolite with Three-Dimensional Intersecting Straight-Channel System of 12-Membered Rings. *J. Am. Chem. Soc.* **2001**, *123*, 5370–5371.
27. Liu, Z.; Yanagi, K.; Suenaga, K.; Kataura, H.; Iijima, S. Imaging the Dynamic Behaviour of Individual Retinal Chromophores Confined Inside Carbon Nanotubes. *Nat. Nanotechnol.* **2007**, *2*, 422–425.
28. Allinger, N. L. Conformational Analysis. 130. MM2. A Hydrocarbon Force Field Utilizing V1 and V2 Torsional Terms. *J. Am. Chem. Soc.* **1977**, *99*, 8127–8134.
29. Lii, J.; Gallion, S.; Bender, C.; Wikstrom, H.; Allinger, N. L.; Flurchick, K. M.; Teeter, M. M. Molecular Mechanics (MM2) Calculations on Peptides and on the Protein Crambin Using the CYBER 205. *J. Comput. Chem.* **1989**, *10*, 503–513.